

Direct observation of valley-hybridization and universal symmetry of graphene with mesoscopic conductance fluctuations

Atindra Nath Pal, Vidya Kochat, and Arindam Ghosh

Department of Physics, Indian Institute of Science, Bangalore 560 012, India

Abstract

In graphene, the valleys represent spin-like quantities and can act as a physical resource in valley-based electronics to novel quantum computation schemes. Here we demonstrate a direct route to tune and read the valley quantum states of disordered graphene by measuring the mesoscopic conductance fluctuations. We show that the conductance fluctuations in graphene at low temperatures are reduced by a factor of four when valley triplet states are gapped in the presence of short range potential scatterers at high carrier densities. We also show that this implies a gate tunable universal symmetry class which outlines a fundamental feature arising from graphene's unique crystal structure.

Quantum interference of electrons (or holes) causes the electrical conductance G of a disordered metal to fluctuate aperiodically yet reproducibly with Fermi energy, magnetic field or disorder configuration [1–3]. When the sample size is smaller than the phase coherence length (L_ϕ), the conductance fluctuates with a universal magnitude $\sim e^2/h$, the quantum of conductance, irrespective of material properties, device geometry or dimensionality. In conventional mesoscopic conductors, such as thin metal films [1] or weakly localized semiconductor devices [4], both universal conductance fluctuations (UCF) and weak localization effects are well-understood on the common platform of coherent backscattering of quasiparticle wave functions [2].

The scenario is considerably more complex in graphene due to the existence of two degenerate valleys [5]. The hexagonal lattice structure of graphene contains two basis atoms in its unit cell, which makes the conduction and valence bands of graphene cross the Fermi level at two inequivalent K and K' points on the opposite corners of the hexagonal Brillouin zone, leading to two valleys [6, 7]. Consequently, quantum correction to the conductivity in graphene is determined not by the inelastic processes alone, but also by elastic collision events that involve the intervalley and intravalley scattering [8–10].

TABLE I: Details of the single layer graphene devices

Device	Device area (L×W) ¹	Dirac point ²	electron mobility ³	hole mobility ³
Dev I	2.1×2.9	-5.5	12,000	10,000
Dev II	2.5×3.6	-8	4,500	5,700
Dev III	3.3×5.5	40	2,300	2,800

¹ both dimensions in μm

² in Volt

³ in cm^2/Vs at 4 K

Although the signature of UCF in low temperature electrical transport in mesoscale graphene has been reported in numerous experiments [11–14], a quantitative influence of valleys on UCF has never been observed. Numerical investigations suggest that the UCF magnitude in graphene should be stronger than in normal metal, raising doubts whether its

magnitude is “universal” at all [15]. Moreover, UCF is sensitive to the universal symmetry class of a disordered system which in case of graphene is determined by time reversal symmetry (TRS) as well as valley degeneracy [8, 16, 17]. Thus UCF may reveal, for example, whether graphene belongs to the symplectic symmetry class in the absence of intervalley scattering, or whether time reversal symmetry is broken by ripples due to substrate roughness [18], or edge magnetism [19] *etc.*.

In this letter we present the first direct manifestation of the valley coherent states on UCF in monolayer disordered graphene. The key result is the suppression of UCF magnitude within individual phase coherent boxes by a factor of four as the carrier density is increased from close to the Dirac point, where both valley singlet and triplets contribute to the fluctuations, to the high electron or hole density regime, where short range potential fluctuations allow only valley singlets to survive. We find the factor of four suppression to be universal, irrespective of the geometry, carrier mobility or temperature, indicating it to be a unique and fundamental property of mesoscopic graphene.

Graphene devices were prepared by standard micro-mechanical exfoliation of natural graphite on 300 nm $\text{SiO}_2/\text{Si}^{++}$ wafer surface (see the SEM image of a typical graphene device in the inset of Fig. 1a and our earlier works [20] for more detail on device fabrication). Here we present detailed studies on three monolayer graphene devices with varying disorder (see Table I for details). The conventional magnetotransport was studied first, where we used the method described in Ref. [9] to calculate the average magnetoconductance (MC) within small gate voltage (V_{BG}) windows of 4 V for each transverse magnetic field (B). In Fig. 1b we show the quantum correction to conductivity $\Delta\sigma(B) = \sigma(B) - \sigma(0)$, as a function of B in Dev I at three values of V_{BG} which are identified on the resistance, $R - V_{BG}$ trace for the same device in Fig. 1a. Measurements were performed in two terminal configuration as appropriate for UCF [21], although, for fitting the B -dependence of MC we have used the four-terminal resistivity to eliminate the contact resistance. With decreasing density (moving from region 3 to region 1) MC changes its sign from positive to negative similar to the observations in Ref. [10]. This transition from weak localization to weak anti-localization indicates that the scattering associated with short-range defects is stronger at high carrier density and one can tune the relative strength of the elastic scattering just by changing the carrier density or gate voltage. On fitting the traces with the theoretical expression [22], we find that L_ϕ saturates to a value that is in the order of the device dimension in all cases

below ~ 4 K, which is about 5 – 10 times longer than the elastic mean free path [23].

In order to evaluate the magnitude of conductance fluctuations, we chose successive gate voltage windows (of equal width $\Delta V_{BG} = 4$ V) within which the average conductance does not vary appreciably, but we have significant fluctuations for statistically meaningful analysis (up to ~ 800 realizations). The conductance variation within a typical window is shown in Fig. 1c, where the random yet reproducible fluctuations in G has an amplitude of $\sim e^2/h$, which is the hallmark of UCF. The fluctuations weaken with increasing temperature (T), as illustrated in Fig. 1d. Below ~ 300 mK, $\langle \delta G^2 \rangle$ becomes nearly constant as L_ϕ itself saturates to \sim device dimension [23].

In order to establish the origin of the conductance fluctuations, we measured the fluctuation magnitude in a small transverse magnetic field. In Fig. 2 the variation in the normalized noise magnitude $N(B) = \langle \delta G(B)^2 \rangle / \langle G \rangle^2$ with B is shown for Dev III at three values of V_{BG} extending from the Dirac region to high carrier densities (see inset). In all cases $N(B)$ decreases by \sim factor of *two*, as B exceeds ~ 10 mT which is also the characteristic field scale associated with the quantum correction to conductivity ($B_\phi = h/eL_\phi^2 \approx 1 - 4$ mT for Dev III). In the diagrammatic representation of quantum transport, this can be readily explained by the suppression of the Cooperon (particle-particle channel) contribution to UCF for $B \gg B_\phi$, while the diffuson (particle-hole channel) contribution, which is equal in magnitude, remains unaffected [2, 24]. This result has two important implications: First, in the framework of the random matrix theory, the factor of two reduction in UCF can be understood by a B -induced lifting of TRS that drives the system from orthogonal or symplectic symmetry class to the unitary class [3]. Similar observation here indicates that at $B = 0$ there is no spontaneous breaking of TRS in our graphene devices. Second, we conclude that the observed V_{BG} -dependent fluctuation in G is entirely due to UCF, and hence the measured magnitude of $\langle \delta G^2 \rangle$ can be directly used to probe the valley effects and symmetry class of graphene.

Since valley degeneracy is connected to the carrier density through the nature of potential scattering [5, 8, 22], we subsequently measured $\langle \delta G^2 \rangle$ over a wide range of carrier density in all three devices at $T = 10$ mK and $B = 0$. Fig. 3a shows the variation of $\langle \delta G^2 \rangle$ with V_{BG} for Dev I, indicating a weak increase on both sides of the Dirac point. The variation of $\langle \delta G^2 \rangle$ with V_{BG} was found to be highly device specific, with opposing trends observed in different devices [23]. The measured $\langle \delta G^2 \rangle$ however arises from the entire sample, and in order to

estimate the UCF magnitude $\langle \delta G_\phi^2 \rangle$ within a single phase coherent box ($L_\phi \times L_\phi$), we have employed the theorem of classical superposition [2], $\langle \delta G^2 \rangle / \langle G \rangle^2 = (1/N) \times \langle \delta G_\phi^2 \rangle / \langle G_\phi \rangle^2$, where $N = LW/L_\phi^2$ is the number of phase coherent boxes in a device of length L and width W . Using $\langle G_\phi \rangle = \sigma$, the conductivity and $\langle G \rangle = L\sigma/W$, we get,

$$\langle \delta G_\phi^2 \rangle = \frac{L^3}{W} \times \frac{\langle \delta G^2 \rangle}{L_\phi^2}. \quad (1)$$

In Eq. 1, both $\langle \delta G^2 \rangle$ and L_ϕ are V_{BG} -dependent quantities, and we evaluated them experimentally to extract the V_{BG} -dependence of $\langle \delta G_\phi^2 \rangle$. Fig. 3b shows the dependence of L_ϕ with V_{BG} in Dev I over the same range of V_{BG} . L_ϕ increases with increasing density, and near the Dirac region it shows a minimum. This is typical for graphene and could be connected to dominance of electron-electron scattering with increasing densities [25]. In Fig. 3c we have shown the variation of $\langle \delta G_\phi^2 \rangle$ with V_{BG} in Dev I at $B = 0$, using experimentally measured $\langle \delta G^2 \rangle$ and L_ϕ (from MC) at every gate voltage. While the absolute magnitude of $\langle \delta G_\phi^2 \rangle$ is expectedly of the order of $(e^2/h)^2$ in all cases, the key aspect is the suppression of $\langle \delta G_\phi^2 \rangle$ by a factor of ≈ 4 as V_{BG} is varied from the Dirac point towards both high electron or hole density regime. The characteristic scale of such a suppression seems to follow the crossover of linear (Coulomb scattering) to sub-linear (short-range scattering) [26] density-dependence of conductivity (see Fig. 3c and 3d, and vertical guidelines). Similar reductions were observed in the other two devices (Dev II and Dev III) as well, shown in Fig. 4a-d. The suppression of noise is often asymmetric about the Dirac point, probably connected to the difference in mobility and disorder between the electron and hole side.

TABLE II: Values of the symmetry parameters k , s , β for different universality class in case of graphene.

	Density	s			k	β	$\frac{ks^2}{\beta}$	Universality class
		valley-isospin	Kramer's degeneracy	real spin				
B = 0 T	$n \rightarrow \text{low}$	2	2	2	1	4	16	GSE
	$n \rightarrow \text{high}$	1	1	2	1	1	4	GOE
B = 100 mT	$n \rightarrow \text{low}$	2	1	2	1	2	8	GUE
	$n \rightarrow \text{high}$	1	1	2	1	2	2	GUE

The factor of four suppression in $\langle \delta G_\phi^2 \rangle$, irrespective of mobility, geometry and other device specific details, suggests a fundamental property of disordered graphene. In a recent

analytical approach, removal of valley degeneracy has been shown to cause an exact factor of four reduction in the mesoscopic fluctuations in graphene [5]. The underlying physical mechanism can be schematically presented as in Fig. 4e. At lower density, the scattering is dominated by the long range Coulomb scattering where the effective valley-isospin rotational symmetry (SRS) is preserved. Consequently, the mesoscopic fluctuations receive equal contribution from each of the singlet and (three) triplet channels of diffusons and Cooperons. However, at higher densities the intervalley scattering dominates, and the effective SRS is lifted, and only the singlet diffuson and Cooperon channels contribute. In the latter case the graphene essentially behaves as a conventional 2D disordered metal.

The existence of valleys is also expected to result in a nontrivial symmetry property of graphene Hamiltonian that has never been probed in a direct manner. At zero magnetic field the presence of valley isospin rotational symmetry (no intervalley scattering) makes graphene belong to the Gaussian symplectic ensemble (GSE), characterized by a Wigner-Dyson parameter $\beta = 4$, and doubly degenerate isospin and effective time reversed states (Kramer's degeneracy). Removal of valley degeneracy results in a Gaussian orthogonal ensemble (GOE) with $\beta = 1$ as well as suppression of effective Kramer's degeneracy [16]. For open mesoscopic systems, the random matrix theory connects the magnitude of UCF to its symmetry class simply as [3],

$$\langle \delta G_\phi^2 \rangle \approx \left(\frac{e^2}{h} \right)^2 \frac{k s^2}{\beta} \quad (2)$$

where k is the number of independent eigenvalue sequences of the transmission matrix or Hamiltonian, s is the eigenvalue degeneracy. As shown in the first row of Table II, factor of four suppression of UCF with increasing carrier density can be explained from the change in symmetry properties of graphene as the valley degeneracy is removed.

Finally, in order to establish the consistency of Eq. 2, we have measured the V_{BG} dependence of $\langle \delta G_\phi^2 \rangle$ at a finite B ($\gg \frac{h}{eL_\phi^2}$), which removes the time reversal symmetry and puts graphene in the Gaussian unitary ensemble (GUE, $\beta = 2$) at all densities. As shown for Dev III at different temperatures (Fig. 5), $\langle \delta G_\phi^2 \rangle$ is again suppressed by a factor of four at high densities irrespective of T , which can be understood either as gapping of triplet diffusons, or alternatively as, suppression of valley isospin degeneracy in Eq. 2 (see lower row of Table II).

In conclusion, we have demonstrated for the first time that the mesoscopic conductance

fluctuations in single layer graphene are dependent on the valley hybridized states and physical symmetries of Hamiltonian. We have shown that the variance of universal conductance fluctuations can be a sensitive probe to this, which in a single phase coherent box increases by four times near the Dirac region as compared to high density. This sensitivity could be exploited in read-out schemes involving valley states in graphene.

Acknowledgement: We thank Carlo Beenakker and G. Baskaran for useful discussions. We acknowledge the Department of Science and Technology (DST) for a funded project. ANP and VK thank CSIR for financial support.

-
- [1] N. O. Birge, B. Golding, and W. H. Haemmerle, Phys. Rev. Lett. **62**, 195 (1989).
 - [2] S. Feng, P. A. Lee, and A. D. Stone, Phys. Rev. Lett. **56**, 1960 (1986).
 - [3] B. L. Al'tshuler and B. Shklovskii, JETP Lett. **64**, 127 (1986).
 - [4] A. Ghosh and A. K. Raychaudhuri, Phys. Rev. Lett. **84**, 4681 (2000).
 - [5] M. Y. Kharitonov and K. B. Efetov, Phys. Rev. B **78**, 033404 (2008).
 - [6] P. R. Wallace, Phys. Rev. **71**, 622 (1947).
 - [7] A. H. Castro Neto, F. Guinea, N. M. R. Peres, K. S. Novoselov, and A. K. Geim, Rev. Mod. Phys. **81**, 109 (2009).
 - [8] S. Das Sarma, S. Adam, E. H. Hwang, and E. Rossi, Rev. Mod. Phys. **83**, 407 (2011).
 - [9] F. V. Tikhonenko, D. W. Horsell, R. V. Gorbachev, and A. K. Savchenko, Phys. Rev. Lett. **100**, 056802 (2008).
 - [10] F. V. Tikhonenko, A. A. Kozikov, A. K. Savchenko, and R. V. Gorbachev, Phys. Rev. Lett. **103**, 226801 (2009).
 - [11] D. Horsell, A. Savchenko, F. Tikhonenko, K. Kechedzhi, I. Lerner, and V. Falko, Solid State Commun. **149**, 1041 (2009).
 - [12] Y.-F. Chen, M.-H. Bae, C. Chialvo, T. Dirks, A. Bezryadin, and N. Mason, Journal of Physics: Condensed Matter **22**, 205301 (2010).
 - [13] J. Berezovsky, M. F. Borunda, E. J. Heller, and R. M. Westervelt, Nanotechnology **21**, 274013 (2010).
 - [14] M. F. Borunda, J. Berezovsky, R. M. Westervelt, and E. J. Heller, ACS Nano **5**, 3622 (2011).
 - [15] A. Rycerz, J. Tworzydo, and C. W. J. Beenakker, EPL **79**, 57003 (2007).

- [16] H. Suzuura and T. Ando, Phys. Rev. Lett. **89**, 266603 (2002).
- [17] D. Xiao, W. Yao, and Q. Niu, Phys. Rev. Lett. **99**, 236809 (2007).
- [18] A. F. Morpurgo and F. Guinea, Phys. Rev. Lett. **97**, 196804 (2006).
- [19] S. Bhowmick and V. B. Shenoy, J. Chem. Phys. **128**, 244717 (2008).
- [20] A. N. Pal and A. Ghosh, Phys. Rev. Lett. **102**, 126805 (2009); A. N. Pal and A. Ghosh, Appl. Phys. Lett. **95**, 082105 (2009); A. N. Pal, S. Ghatak, V. Kochat, E. S. Sneha, A. Sampathkumar, S. Raghavan, and A. Ghosh, ACS Nano **5**, 2075 (2011).
- [21] P. A. Lee, A. D. Stone, and H. Fukuyama, Phys. Rev. B **35**, 1039 (1987).
- [22] E. McCann, K. Kechedzhi, V. I. Fal'ko, H. Suzuura, T. Ando, and B. L. Altshuler, Phys. Rev. Lett. **97**, 146805 (2006).
- [23] See supplementary online material.
- [24] A. D. Stone, Phys. Rev. B **39**, 10736 (1989).
- [25] D.-K. Ki, D. Jeong, J.-H. Choi, H.-J. Lee, and K.-S. Park, Phys. Rev. B **78**, 125409 (2008).
- [26] E. H. Hwang, S. Adam, and S. Das Sarma, Phys. Rev. Lett. **98**, 186806 (2007).

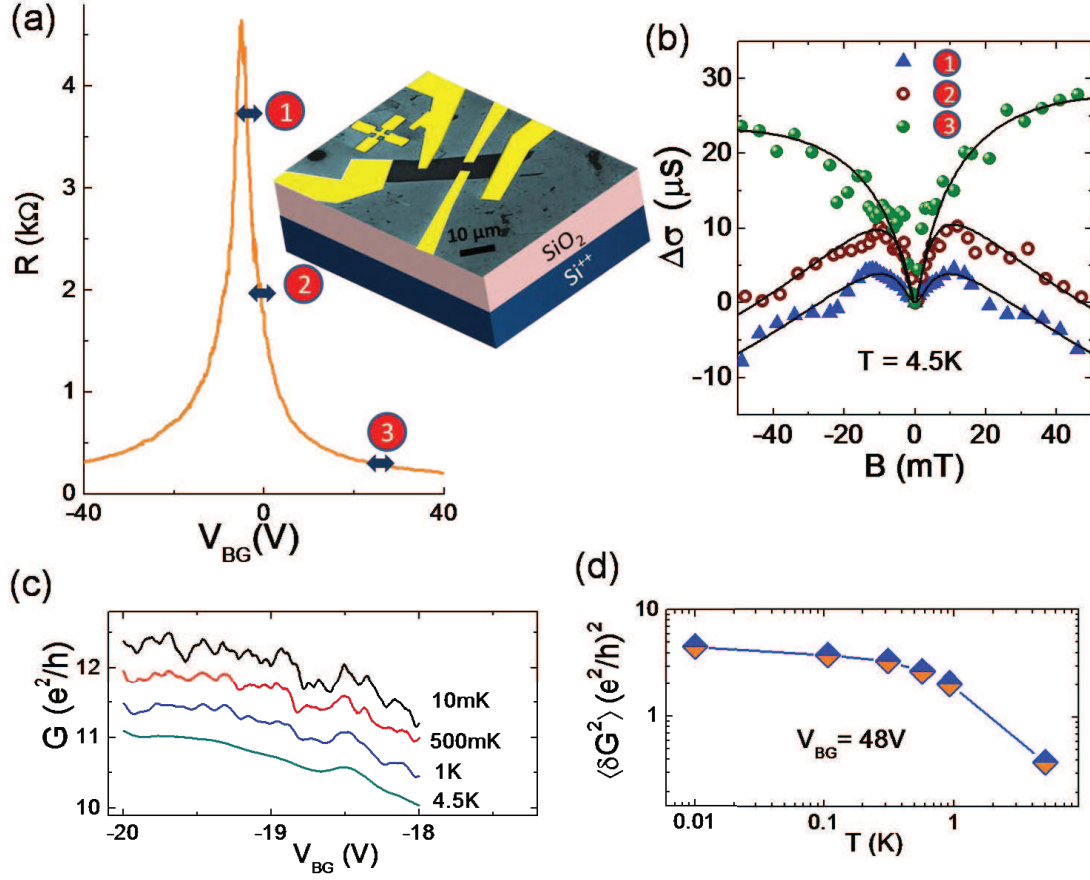


Figure 1

FIG. 1: (color online). (a) Resistance (R) vs. gate voltage (V_{BG}) characteristics for a single layer device (Dev I) at $T = 10$ mK. Inset shows the schematic along with the false color SEM image of a typical graphene transistor. (b) Evolution of Magnetoconductance with increasing electron density measured at $T = 4.5$ K. Solid lines are fit to the weak localization theory [22, 23]. (c) Conductance fluctuations as a function of gate voltage for Dev I, shown for various temperatures. Curves at different temperatures are shifted for clarity. (d) Variance in conductance, calculated from the conductance fluctuations in gate voltage range -50 V to -46 V for Dev I, plotted as a function of temperature.

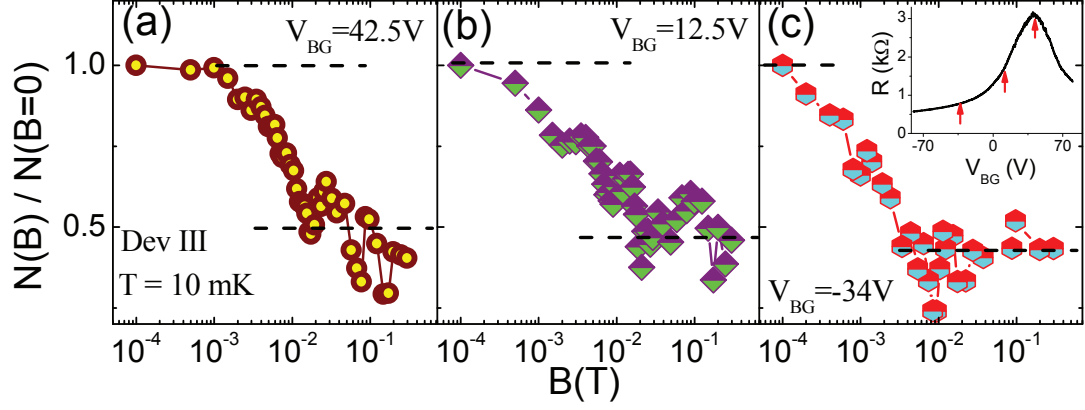


Figure 2

FIG. 2: (color online). Magnetic field dependence of the magnitude of conductance fluctuations for Dev III at $T = 10$ mK at various gate voltages: (a) 42.5 V, (b) 12.5 V, and (c) -34 V. For comparison, we have plotted the ratio $N(B)/N(B=0)$, with $N(B) = \langle \delta G^2 \rangle / \langle G \rangle^2$ at the magnetic field B . Inset shows the $R - V_{BG}$ characteristics of Dev III at $T = 10$ mK with arrows indicating the three measured regions.

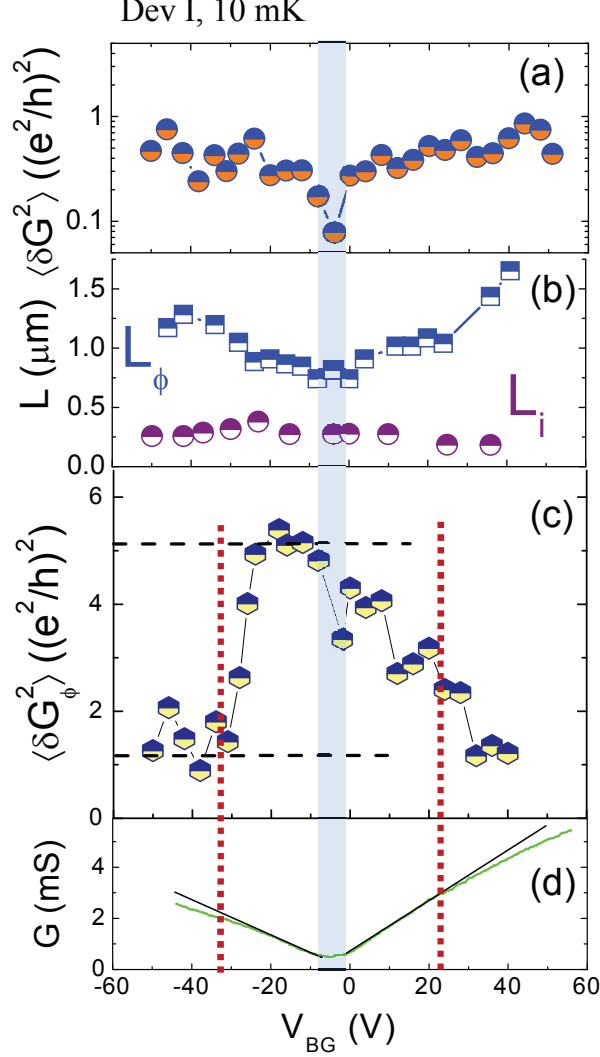


Figure 3

FIG. 3: (color online). (a) Variance in conductance ($\langle \delta G^2 \rangle$) vs. gate voltage (V_{BG}) at 10 mK for Dev I. (b) Gate voltage dependence of L_ϕ and L_i at $T = 10$ mK, extracted from the weak localization fits, are shown for Dev I. (c) The variance in conductance in a phase coherent box of area L_ϕ^2 , $\langle \delta G_\phi^2 \rangle$, extracted from (a) and (b), is plotted with gate voltage for Dev I. The factor of four is indicated by the dashed lines. (d) Conductance (G) vs. gate voltage (V_{BG}) for the device at $T = 10$ mK. The solid line indicates the linear region in both electron and hole sides. The vertical dotted lines in (c) and (d) indicate the densities where the short-range scattering dominate. The shaded region indicates the inhomogeneous region near the Dirac point.

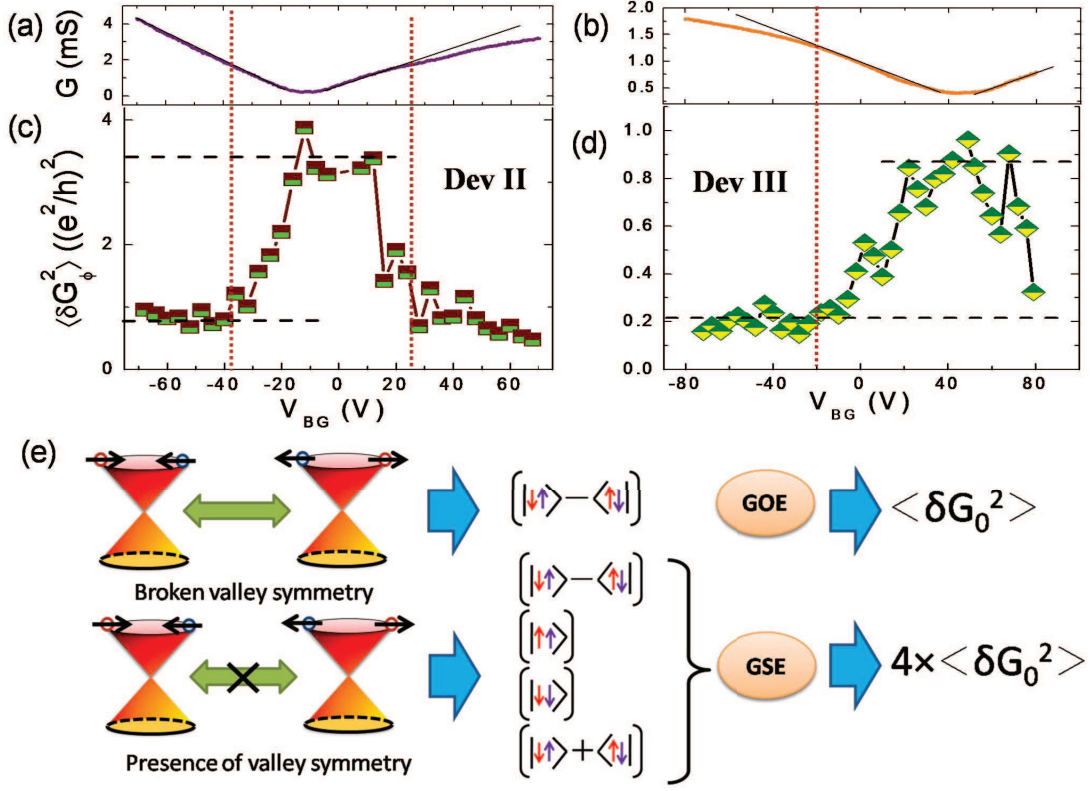


Figure 4

FIG. 4: (color online). (a)-(b) Conductance (G) vs. gate voltage (V_{BG}) at 10 mK for Dev II and Dev III, respectively. The solid line indicates the linear region in both electron and hole sides. (c)-(d) The variance from conductance fluctuations in a phase coherent box of area L_ϕ^2 is plotted with gate voltage for Dev II and III, see details in Table I. The factor of four is indicated by the dashed lines. The vertical dotted lines indicate the densities beyond which the short-range scattering dominates. (e) Schematic describing the crossover from orthogonal to symplectic universality class depending on the presence of short range scattering which breaks the effective valley-isospin rotational symmetry with $\langle \delta G_0^2 \rangle$ being the variance in conductance for a single phase coherent box at very high density.

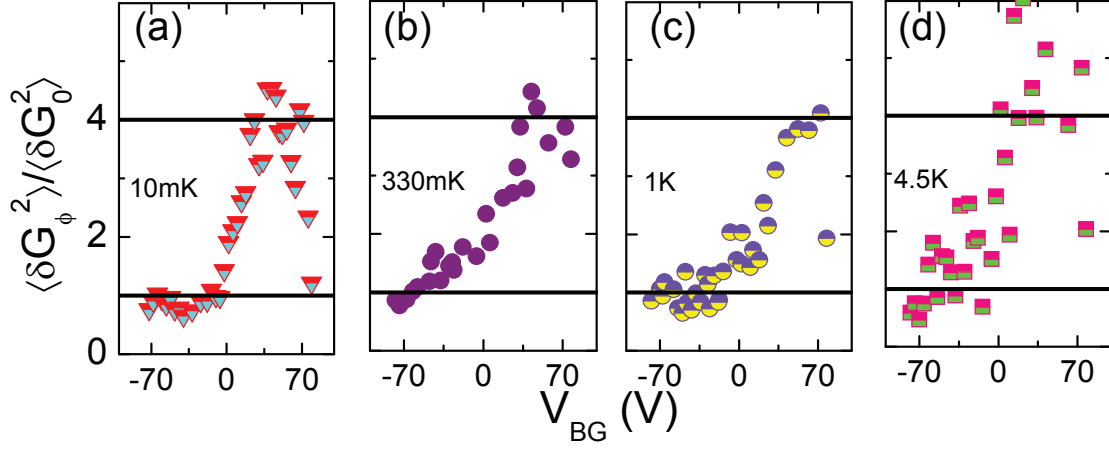


Figure 5

FIG. 5: (color online). (a)-(d) Gate voltage dependence of the ratio $\langle \delta G_\phi^2 \rangle / \langle \delta G_0^2 \rangle$ for Dev III, plotted for various temperatures at $B = 100$ mT, where $\langle \delta G_0^2 \rangle$ is the variance in the conductance for a single phase coherent box at $V_{BG} = -68$ V.

Supplementary Information

Direct observation of valley-hybridization and universal symmetry of graphene with mesoscopic conductance fluctuations

Atindra Nath Pal, Vidya Kochat, and Arindam Ghosh
Department of Physics, Indian Institute of Science,
Bangalore 560 012, India.

MAGNETOCONDUCTIVITY MEASUREMENTS

For magnetoconductivity (MC) measurements we have averaged out the fluctuations over a gate voltage window of $\Delta V_{BG} = 4$ V, following Ref. [1], to get the conductivity correction $\Delta\sigma = \langle\sigma(V_{BG}, B) - \sigma(V_{BG}, 0)\rangle_{\Delta V_{BG}}$. The quantum correction depends not only on the dephasing rate τ_ϕ^{-1} , but also intervalley (τ_i^{-1}) and intravalley scattering rate (τ_*^{-1}). To fit the MC data we have used the weak localization theory for graphene, given in Ref. [2],

$$\Delta\sigma(B) = \frac{e^2}{\pi h} \left(F\left(\frac{\tau_B^{-1}}{\tau_\phi^{-1}}\right) - F\left(\frac{\tau_B^{-1}}{\tau_\phi^{-1} + 2\tau_i^{-1}}\right) - 2F\left(\frac{\tau_B^{-1}}{\tau_\phi^{-1} + \tau_i^{-1} + \tau_*^{-1}}\right) \right). \quad (1)$$

Here, $F(z) = \ln z + \psi(0.5 + z^{-1})$, $\psi(x)$ is the digamma function, $\tau_B^{-1} = 4eDB/\hbar$ [D is the diffusion constant]. The diffusion constant, $D = v_F l/2$, was determined from the mean free path $l = \hbar/2e^2 k_F \rho$, where ρ is the four terminal resistivity at that gate voltage. The corresponding scattering lengths can be calculated using the formula, $L_{\phi,i,*} = \sqrt{D\tau_{\phi,i,*}}$.

Temperature dependence of scattering lengths

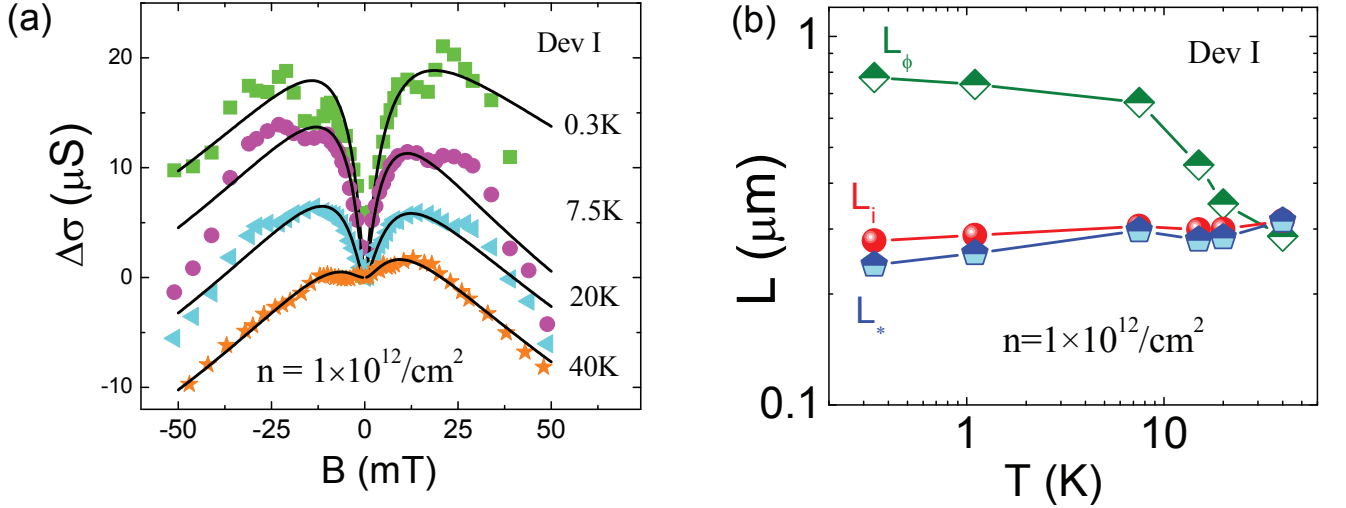


Fig. S1. (a) Magnetoconductivity as a function of temperature taken at an electron density $n = 1 \times 10^{12}/\text{cm}^2$. Solid lines are fit to the weak localization theory (Eq. 1). (b) The scattering length scales as a function of temperature, extracted from the fits.

Fig. S1a shows the MC data at a particular density ($1 \times 10^{12}/\text{cm}^2$) for various temperatures for Dev I and the corresponding fits are shown by solid black lines. With increasing temperature the inelastic phase coherence length (L_ϕ) decreases (Fig. S1b) and saturates at lower temperatures ($\lesssim 4$ K) at this particular carrier density. However, the intervalley and intravalley scattering lengths remain almost constant with temperature as these are related to the elastic scattering [2, 3].

Gate voltage dependence of L_ϕ and L_i

Fig. S2a and S2b show the gate voltage/density dependence of MC data at the base temperature of ~ 10 mK for Dev II and Dev III, respectively. It is clear from both the graphs that with increasing density L_ϕ increases, whereas, the intervalley scattering length (L_i) remains unchanged. The density dependence of the scattering lengths have been studied in detail in Ref. [4]. To calculate the fluctuations from a single phase coherent box we have divided the area between the voltage probes in small boxes of area L_ϕ^2 , schematically shown in Fig. S2c. We have used the L_ϕ value for a particular density, extracted from the fits.

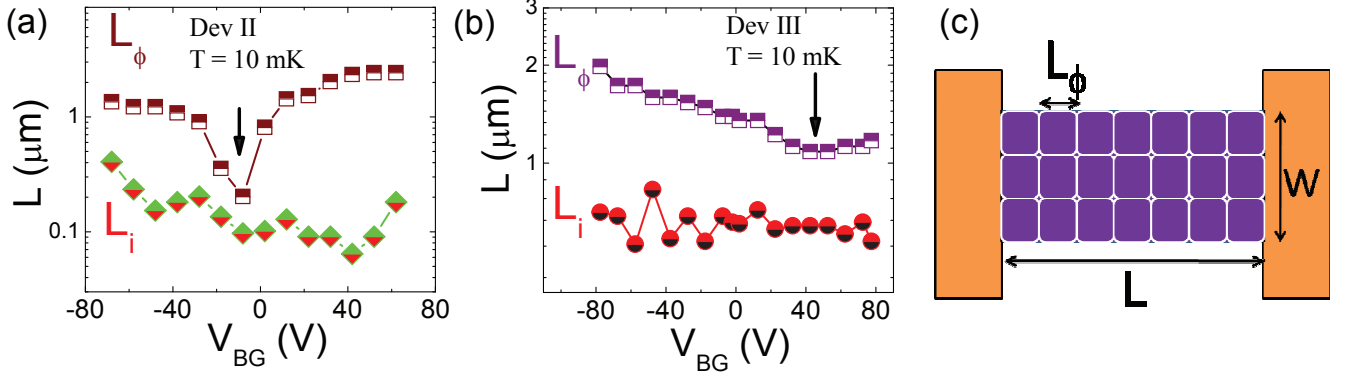


Fig. S2. Gate voltage dependence of L_ϕ and L_i at $T = 10$ mK, extracted from the weak localization fits, are shown for (a) Dev II and (b) Dev III. (c) Schematic describing that the area ($L \times W$) between the voltage probes can be divided into phase coherent boxes of area L_ϕ^2 .

GATE VOLTAGE DEPENDENCE OF $\langle \delta G^2 \rangle$

Fig. S3a and S3b shows the variation of $\langle \delta G^2 \rangle$ with gate voltage for Dev II and Dev III, respectively. $\langle \delta G^2 \rangle$ was calculated using the formula $\langle \delta G^2 \rangle = \langle \delta R^2 \rangle / \langle R \rangle^4$, where $\langle R \rangle$ is the average four terminal resistance in that gate voltage window. We observe that $\langle \delta G^2 \rangle$ is very much device specific and hence, is not a significant parameter to understand the absolute magnitude of UCF.

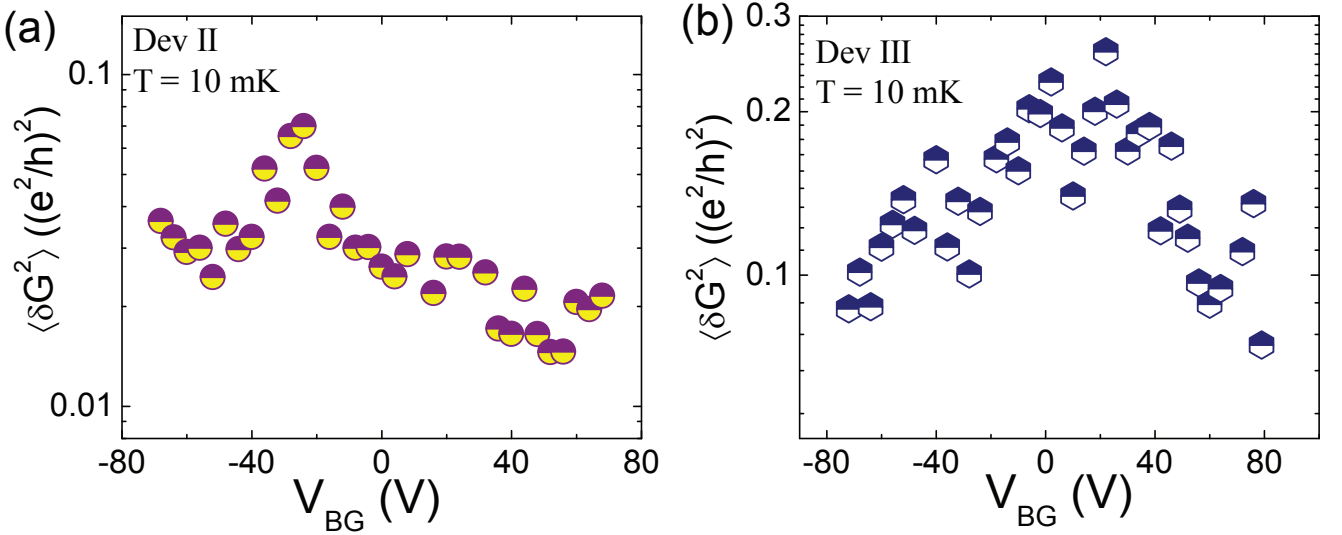


Fig. S3. Variation of $\langle \delta G^2 \rangle$ with gate voltage at $T = 10$ mK, for (a) Dev II and (b) Dev III.

-
- [1] F. V. Tikhonenko, A. A. Kozikov, A. K. Savchenko, and R. V. Gorbachev, Phys. Rev. Lett. **103**, 226801 (2009).
 - [2] E. McCann, K. Kechedzhi, V. I. Fal'ko, H. Suzuura, T. Ando, and B. L. Altshuler, Phys. Rev. Lett. **97**, 146805 (2006).
 - [3] F. V. Tikhonenko, D. W. Horsell, R. V. Gorbachev, and A. K. Savchenko, Phys. Rev. Lett. **100**, 056802 (2008).
 - [4] D.-K. Ki, D. Jeong, J.-H. Choi, H.-J. Lee, and K.-S. Park, Phys. Rev. B **78**, 125409 (2008).